

Higgs Boson Production in Association with a Photon in Vector Boson Fusion at the LHC

Emidio Gabrielli¹, Fabio Maltoni², Barbara Mele³,
Mauro Moretti⁴, Fulvio Piccinini⁵, and Roberto Pittau⁶

¹*Helsinki Institute of Physics, POB 64, University of Helsinki, FIN 00014, Finland*

²*Centre for Particle Physics and Phenomenology (CP3)*

Université catholique de Louvain

Chemin du Cyclotron 2, B-1348 Louvain-la-Neuve, Belgium

³*INFN, Sezione di Roma, and Dipartimento di Fisica, Università La Sapienza,
P.le A. Moro 2, I-00185 Rome, Italy*

⁴*Dipartimento di Fisica Università di Ferrara, and INFN, Sezione di Ferrara,
via Saragat 1, I 44100, Ferrara, Italy*

⁵*INFN, Sezione di Pavia, via A. Bassi 6, I 27100, Pavia, Italy*

⁶*Dipartimento di Fisica Teorica, Università di Torino, and INFN sezione di Torino,
via P. Giuria 1, Torino, Italy*

Abstract

Higgs boson production in association with two forward jets and a central photon at the CERN Large Hadron Collider is analyzed, for the Higgs boson decaying into a $b\bar{b}$ pair in the $m_H \lesssim 140$ GeV mass region. We study both irreducible and main reducible backgrounds at parton level. Compared to the Higgs production via vector-boson fusion, the request of a further photon at moderate rapidities dramatically enhances the signal/background ratio. Inclusive cross sections for $p_T^\gamma \gtrsim 20$ GeV can reach a few tens of fb's. After a suitable choice of kinematical cuts, the cross-section ratio for signal and irreducible-background can be enhanced up to $\gtrsim 1/10$, with a signal cross section of the order of a few fb's, for $m_H \sim 120$ GeV. The request of a central photon radiation also enhances the relative signal sensitivity to the WWH coupling with respect to the ZZH coupling. Hence, a determination of the cross section for the associated production of a Higgs boson decaying into a $b\bar{b}$ pair plus a central photon in vector-boson fusion could help in constraining the $b\bar{b}H$ coupling, and the WWH coupling as well. A preliminary study of QCD showering effects points to a further significant improvement of the signal detectability over the background.

1 Introduction

Higgs boson search is one of the main tasks of present and future collider experiments. The Higgs mechanism, responsible for the electroweak symmetry breaking (EWSB) in the Standard Model (SM), predicts the existence of a scalar particle, the Higgs boson, that is still eluding any direct experimental test. The fact that the Higgs boson mass is not predicted in the SM, ranging from the present experimental lower limit of 114 GeV [1], up to the theoretical upper bound of about 800 GeV [2, 3, 4], makes this search more difficult. Despite the large theoretical uncertainty on its mass, present precision tests of electroweak observables indicate that the data consistency in the SM requires a light Higgs [1], that is in a range close to the present experimental lower limit. Moreover, in the minimal supersymmetric extension of the SM the lightest Higgs scalar is expected to be lighter than about 135 GeV [5]. Clearly, the discovery of the Higgs boson would be a fundamental handle in pinpointing the EWSB mechanism, possibly shedding some light on physics scenarios beyond the SM.

Higgs boson production mechanisms at colliders have been intensively analyzed in the literature [6]. The fact that Higgs couplings to particles are proportional to their masses makes Higgs production mechanisms and search strategies quite peculiar. A light Higgs boson (with $m_H \lesssim 135$ GeV) mainly decays into $b\bar{b}$ pairs, making its experimental search very challenging at hadron colliders, because of large backgrounds from QCD b -quark production. At the CERN Large Hadron Collider (LHC), the Higgs boson is expected to be produced with high rate via gluon or vector-boson fusion (VBF) mechanisms and associate $W(Z)H$ production. A possible way to tame the huge QCD background in the search of a light Higgs boson is to look at its rare decays. In particular, the $H \rightarrow \gamma\gamma$ [7], $H \rightarrow \tau\tau$ [8], and $H \rightarrow Z^*Z^* \rightarrow 4\ell$ channels are particularly promising, allowing the observation of the signal in a moderate background environment.

On the other hand, it would be crucial to make at the LHC also a measurement of the $Hb\bar{b}$ coupling [9]. To this aim, Higgs production via VBF, with the Higgs boson decaying into a $b\bar{b}$ pair, has been analyzed in [10]. The VBF characteristic signature is the presence of two forward jets with a typical transverse momentum of the order of M_W , allowing a quite effective reduction of the background. Nevertheless, different sources of QCD backgrounds and hadronic effects, that are hard to control, make the relevance of this channel for a $Hb\bar{b}$ determination presently difficult to assess.

Another potential channel for a $Hb\bar{b}$ coupling measurement is the associated production $Ht\bar{t}$, where the Higgs boson is radiated by a top-quark pair [11, 12]. Unfortunately, recent studies that include a more reliable QCD background estimate and detector simulation, see for instance Ref. [13], have lowered the expectations on the

discovery potential of this channel.

In this paper, we consider a further process that could help in determining the $Hb\bar{b}$ coupling, that is the Higgs boson production in association with a large transverse-momentum photon (with $p_T \gtrsim 20$ GeV) and two *forward* jets

$$pp \rightarrow H \gamma jj \rightarrow b\bar{b} \gamma jj + X, \quad (1)$$

with H decaying to $b\bar{b}$, where at the parton level the final QCD parton is identified with the corresponding jet. The Feynman diagrams that are dominant for this process at the parton level are the ones involving VBF. They are shown in Figure 1, where the Higgs decay to $b\bar{b}$ is not included. In principle, final states $b\bar{b} \gamma jj$ can also arise from photon radiation from one of the two b -quarks coming from the Higgs boson decay, via the process $pp \rightarrow H(\rightarrow b\bar{b} \gamma) jj$. In our study, we will not include the latter set of diagrams, since the requirement of a large p_T photon would shift in that case the $b\bar{b}$ invariant mass outside the experimental $b\bar{b}$ mass resolution window around the Higgs mass. We will then assume that the effect of diagrams with photons arising from the final b 's will vanish after applying the Higgs mass constraint in the event analysis of the $b\bar{b} \gamma jj$ final state.

There is a number of advantages in considering this QED higher-order variant of the VBF Higgs production process $pp \rightarrow H(\rightarrow b\bar{b}) jj$. The fact that the production rate is penalized by the electromagnetic coupling is compensated by a few peculiarities of the channel in Eq. (1).

First of all, the presence of an additional high p_T photon can improve the triggering efficiencies for multi-jet final states, such as those needed to select $pp \rightarrow H(\rightarrow b\bar{b}) jj$ events. Second, there is a large gluonic component entering the partonic processes giving rise to the QCD backgrounds to the $b\bar{b} \gamma jj$ final state. As a consequence, the QCD backgrounds are in general much less *active* in radiating a large p_T photon with respect to the VBF signal. In addition there are further dynamical effects that dramatically suppress the radiation of a central photon in the irreducible QCD background to $b\bar{b} \gamma jj$ with respect to the VBF channel, as we shall see in Section 3.

The requirement of a central photon is also expected to strongly reduce the contribution arising from alternative Higgs boson production processes, such as the one coming from the virtual gluon fusion $g^*g^* \rightarrow H$ diagrams [14], with a photon radiated from any external quark leg*. This expectation is confirmed in our analysis.

The requirement of having two jets with high p_T in the final states also suppresses any contamination from the one-loop $q\bar{q} \rightarrow H\gamma$ process, that has anyhow a quite low cross section at the LHC [15].

*Note that the virtual gluon fusion diagrams $g^*g^* \rightarrow H\gamma$, where a photon is attached to the top-quark loop, exactly vanishes according to charge conjugation invariance.

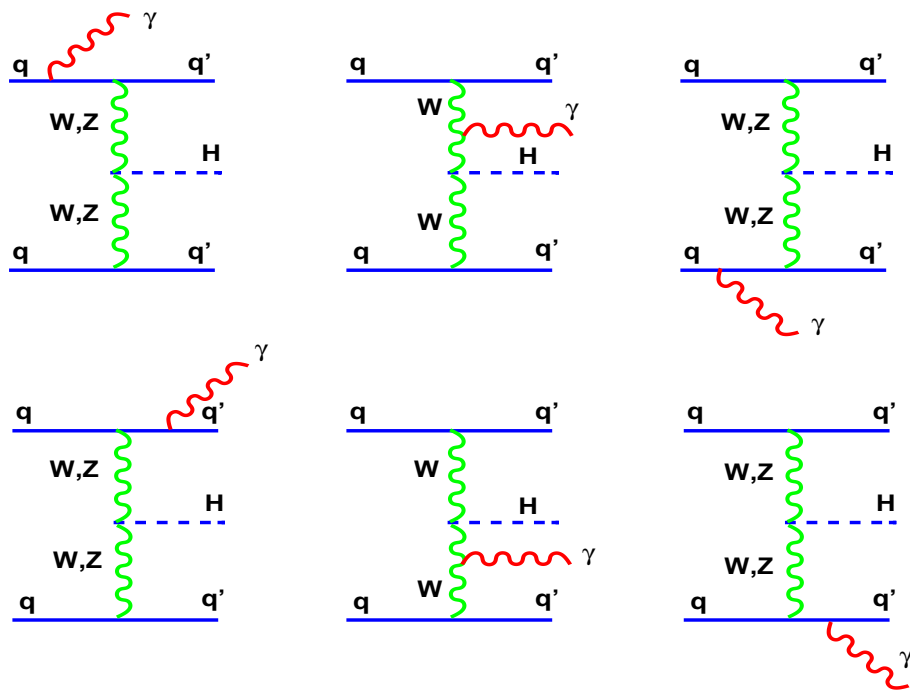


Figure 1: Tree-level t -channel Feynman diagrams for Higgs boson production in the process $pp \rightarrow H \gamma jj$. Here, q and q' stand for different light quarks (u, d, s, c), while $q = q'$ when a Z boson is exchanged.

There is a further issue that increases the potential of the process in Eq. (1) for the determination of Higgs boson couplings. We will see that the requirement of a central photon depletes the HZZ amplitudes with the respect to the HWW ones in Figure 1. As a consequence, the relative sensitivity to the HWW coupling is considerably increased in the radiative channel. Hence, a measurement of the $b\bar{b}\gamma jj$ rate could lead to a combined determination of the Higgs boson couplings to b quarks and W vector bosons, with less contamination from the HZZ coupling uncertainties.

In [16], another method for extracting information on the $H\bar{b}b$ coupling has been suggested through the Higgs boson production in association with a W plus two forward jets. In this case, the main reducible backgrounds are given by the $Wb\bar{b}jj$ and $t\bar{t}jj$ final states, and can be suppressed by proper kinematical cuts. However, the requirement of a leptonic decay of the W limits the event statistics. In the following, we will compare the corresponding rates with the $b\bar{b}\gamma jj$ ones that we analyze here.

The plan of the paper is the following. In Section 2, we go through the main kinematical and dynamical characteristics of the process in Eq. (1). We also discuss the features of the main QCD irreducible background. Section 3 is devoted to the discussion of the destructive quantum interference mechanism that is largely responsible both for the improvement in the signal-to-background ratio of the channel considered, and for its increased sensitivity to the WWH coupling. In Section 4, the signal rates are computed at parton level for a set of kinematical cuts that optimizes the signal/background ratio, restricting the analysis to the case of the irreducible background. Some relevant kinematical distributions are also shown, and compared with the ones for the basic VBF process Hjj . In Section 5, the main reducible background channels are included in the analysis. Some preliminary study of parton-shower effects and jet veto strategies, that turn out to improve the signal detectability, is performed in Section 6. Finally, in Section 7, we draw our conclusions.

2 Signal and irreducible background

Cross sections for the $H\gamma jj$ production at $\sqrt{S} = 14$ TeV are shown in Table 1. In order to present results as inclusive as possible only a minimal set of kinematical cuts is applied ($\Delta R_{\gamma j} > 0.4$, $p_T^\gamma \geq 20$ GeV, and $m_{jj} > 100$ GeV). The cut on the invariant mass of the final quark pair (m_{jj}) avoids the contribution from *resonant* $HW\gamma$, $HZ\gamma$ associated production. The Higgs boson branching ratios to $b\bar{b}$, which are not included in the cross section results, (computed through HDECAY [17]), are also shown. The full tree-level matrix elements for the electroweak process $pp \rightarrow H\gamma jj$ have been computed independently with ALPGEN [18], and MadEvent [19]. Details on the

m_H (GeV)	110	120	130	140
$\sigma(H\gamma jj)$ [fb]	67.4	64.0	60.4	56.1
$\mathcal{BR}(H \rightarrow b\bar{b})$	0.770	0.678	0.525	0.341

Table 1: Cross sections for the $H\gamma jj$ signal at LHC, for $p_T^\gamma \geq 20$ GeV, $\Delta R_{\gamma j} > 0.4$, and a cut $m_{jj} > 100$ GeV on the invariant mass of the final quark pair. Also shown are the Higgs boson branching ratios to $b\bar{b}$ (computed through HDECAY [17]), that are not included in the cross sections shown.

values of the input parameters, such PDF's and scales are given in Section 4.

For comparison, the inclusive $HWjj$ cross section, with a further cut $|m_{ik}^2| > 100 \text{ GeV}^2$ on the invariant mass of any ik initial-final quark pair to avoid singularities due to t -channel virtual photons, is 73 fb, for $m_H = 120$ GeV. Requiring the leptonic (either μ^\pm and e^\pm) signature for the W [16], one ends up with a rate for the $H\gamma jj$ signal of about 4 times the $H\ell\nu jj$ rate, in the relevant m_H range. This factor increases, when more realistic kinematical cuts are applied (see Section 4).

Since the LHC detector capabilities are not completely settled yet, in what follows we will assume two different setups for the high p_T photon threshold: either $p_T^\gamma \geq 20$ GeV or $p_T^\gamma \geq 30$ GeV, the latter being more conservative in the case the photon identification and/or electromagnetic trigger requires a larger photon transverse momentum.

It is useful to recall here the main kinematical properties of a typical VBF event, that is $pp \rightarrow Hjj$, and the corresponding backgrounds, assuming the $H \rightarrow b\bar{b}$ decay, for $m_H \lesssim 140$ GeV. We will see in the next section that the request of a further large p_T photon tends to enhance the peculiar kinematical features of a VBF event. In Figure 2, the basic partonic process for a VBF event, namely $qq \rightarrow qqH$, is shown, where the two final quarks hadronize in two jets. The typical VBF signature consists of two jets with large invariant mass, widely separated in rapidity, and with a typical transverse momentum of $p_T \sim 40$ GeV, the Higgs boson decay products lying at intermediate rapidities. In particular, while one of the two jets is produced quite along the beams, with a pseudorapidity (η) distribution peaked around $\eta \sim 3-4$, the other one is mainly backward, although still in the central detector, with $|\eta| \lesssim 2.5$.

For the Higgs boson decaying to a $b\bar{b}$ pair, the main background to the basic VBF process comes from the QCD production of the final state $b\bar{b}jj$, whenever the $b\bar{b}jj$ kinematical characteristics approach the typical VBF configuration. Here, j stands for a jet originating from either a light quark (u, d, s, c) or a gluon. Seven representative classes for the $b\bar{b}jj$ background Feynman diagrams at parton level are

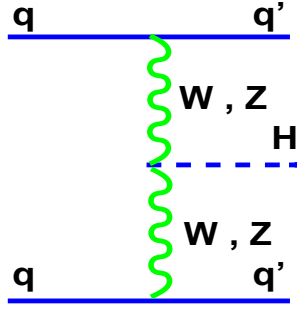


Figure 2: Feynman diagram at parton level for the Higgs boson production via VBF in the process $pp \rightarrow H jj$. Here, q and q' stand for light quarks (u, d, s, c), while $q = q'$ when a Z boson is exchanged.

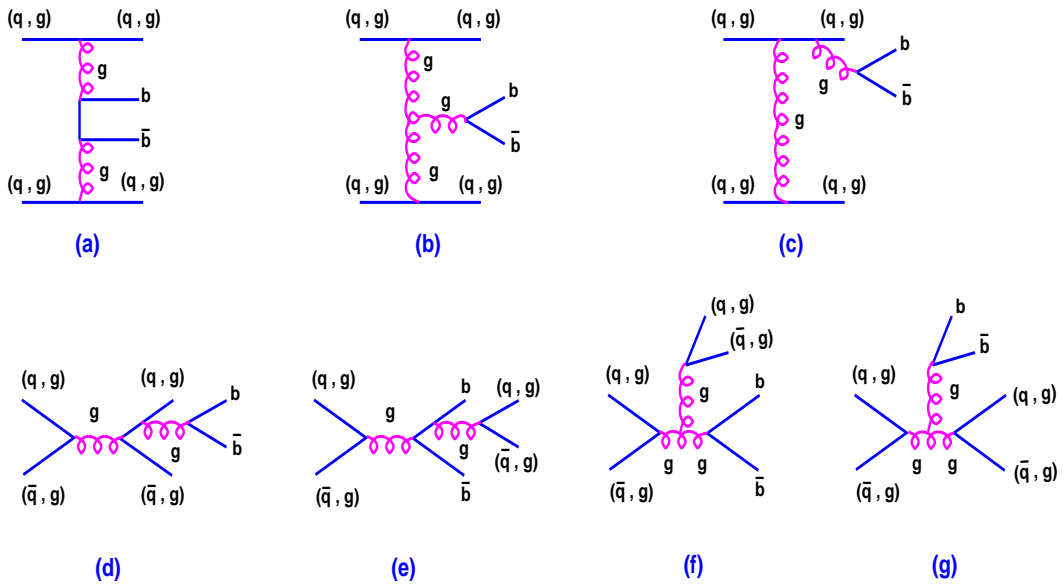


Figure 3: Representative classes of Feynman diagrams contributing, at parton level, to the background process $pp \rightarrow b\bar{b} jj$. Here, q and g stand for a light quark (u, d, s, c) and gluons respectively. The virtual gluon connecting the $b\bar{b}$ pair in $c) - d)$ or the (q, \bar{q}) and (g, g) pairs in $e)$, is understood to be attached in all possible ways to the initial and final parton. Crossed diagrams are not shown.

given in Figure 3 (a–g), where all external partons, but the $b\bar{b}$ final pair, can be either quarks or gluons.

Although the inclusive cross section for the $pp \rightarrow H(\rightarrow b\bar{b})jj$ signal is quite large, of the order of a few pb's, the extraction of the signal from the background is not at all straightforward, being the latter dominant over the signal by a few orders of magnitude. However, with a suitable choice of kinematical cuts, the ratio of the expected signal event number (S) over the background ones (B) can be substantially enhanced. By imposing a large invariant mass cut for the two-forward-jet system [i.e., $m_{jj} \gtrsim \mathcal{O}(1)$ TeV], a minimal p_T^j of a few tens GeV's, and requiring the $b\bar{b}$ invariant mass to be around m_H within the $m_{b\bar{b}}$ experimental resolution, one can obtain a signal significance (S/\sqrt{B}) of the order of $S/\sqrt{B} \sim 3-5$, assuming an integrated luminosity of 600 fb^{-1} [10].

Let us now consider the VBF Higgs production when a further central photon is emitted, namely $pp \rightarrow H \gamma jj$. The Feynman diagrams for the signal in Figure 1 are now to be confronted with the QCD background corresponding to the requirement of a further high p_T photon in the diagrams in Figure 3. For instance, in Figure 4 (a–g), we show the relevant diagrams for one of the leading classes of contributions, i.e. the one related to Figure 3 (a).

According to the usual pattern of QED corrections, one might expect the request of a further hard photon to keep the relative weight of signal and background quite stable. Were this the case, the rates for $pp \rightarrow H \gamma jj$ and its background would be related to a $\mathcal{O}(\alpha)$ rescaling of the rates for the $H jj$ signal and its background, respectively, where α is the fine electromagnetic structure constant. Then, the S/B ratio would not be much affected. On the other hand, both the $H \gamma jj$ signal and its background statistics would decrease according to the rescaling factor $\mathcal{O}(\alpha)$. Consequently, if $(S/\sqrt{B})|_{H(\gamma)jj}$ is the signal significance for the VBF process (with) without a central photon, one would expect the signal significance for $pp \rightarrow H \gamma jj$ to fall down as $(S/\sqrt{B})|_{H\gamma jj} \sim \sqrt{\alpha} (S/\sqrt{B})|_{Hjj} \lesssim 1/10 (S/\sqrt{B})|_{Hjj}$ with respect to the basic VBF process. On this basis, one would conclude that there is no advantage in considering the $H \gamma jj$ variant of the $H jj$ process, apart from the fact that the presence of a hard photon in the final state can improve the triggering efficiency of the detectors.

In the next section, we will show that this pattern does not hold in general. The QED naive expectations definitely hold for inclusive processes, but they do not necessarily apply when restricted regions of phase space are considered. Indeed, we will see that the naive QED rescaling fails for the main background processes considered here, when relevant sets of kinematical cuts are imposed. In particular, the requirement of a further central photon gives rise to a dramatic increase (by more

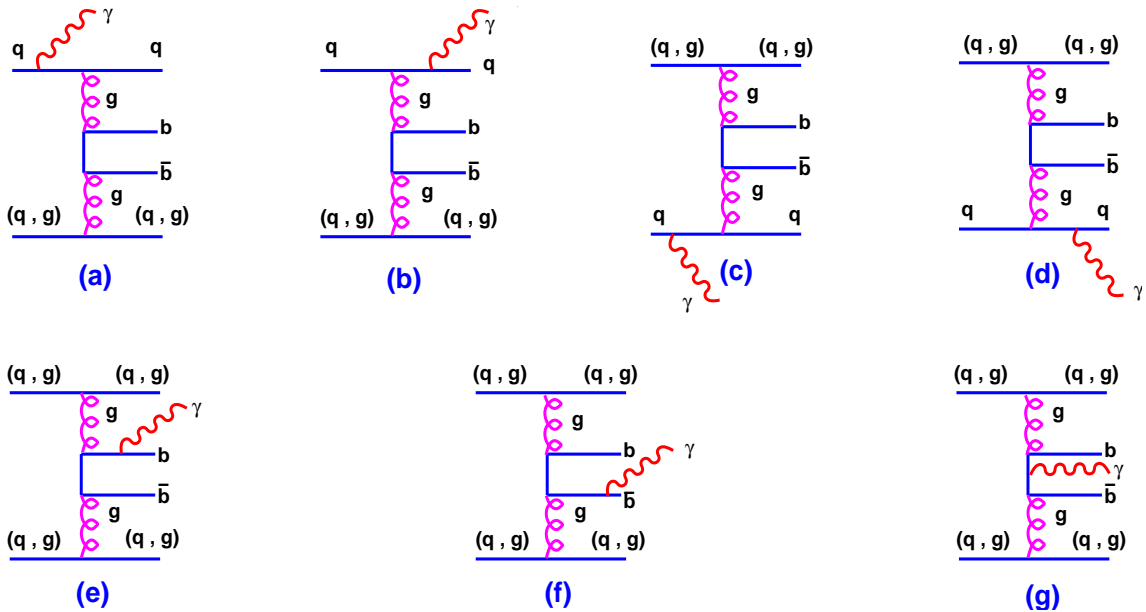


Figure 4: Representative class of Feynman diagrams at parton level for the the background process $pp \rightarrow b\bar{b}jj + \gamma$, corresponding to the photon emission for the class of diagrams in Figure 3 (a). Here q and g stands for a generical light quark (u, d, s, c) and gluon respectively.

than one order of magnitude) in the S/B ratio, while the signal cross section roughly follows the naive QED rescaling.

3 Destructive interferences in central photon emission

We will now go through the main *partonic* components of the irreducible QCD $b\bar{b}jj$ background to the VBF process, in order to study how the request of a further central photon affects each of them, and the overall balance among them.

In our study of the irreducible background, we will not consider the electroweak production of $b\bar{b}jj$ final states (nor its extension to the $b\bar{b}\gamma jj$ case), through, e.g., the mediation of a $Z^{(*)}/\gamma^* \rightarrow b\bar{b}$ decay. The latter contributions have cross sections not much larger than those of the signal considered here (see Section 4, and [10]). On the other hand, their typical $b\bar{b}$ invariant mass is well below the Higgs boson mass range we are considering in the present study. Hence, we do not expect any contamination from this background for the foreseen experimental resolution on $m_{b\bar{b}}$.

In the first two columns of Table 2, we show the absolute (σ_i) and fractional

sub-processes	σ_i (pb)	σ_i/σ	σ_i^γ (fb)	$\sigma_i^\gamma/\sigma^\gamma$
$gq \rightarrow b\bar{b}gq(\gamma)$	57.2(1)	55.3 %	17.3(1)	51.6 %
$gg \rightarrow b\bar{b}gg(\gamma)$	25.2(1)	24.4 %	3.93(3)	11.7 %
$qq' \rightarrow b\bar{b}qq'(\gamma)$	7.76(3)	7.5 %	4.04(2)	12.1 %
$qq \rightarrow b\bar{b}qq(\gamma)$	6.52(2)	6.3 %	4.49(3)	13.4 %
$q\bar{q}' \rightarrow b\bar{b}q\bar{q}'(\gamma)$	4.60(2)	4.4 %	2.28(2)	6.8 %
$q\bar{q} \rightarrow b\bar{b}q\bar{q}(\gamma)$	2.13(2)	2.1 %	1.21(2)	3.6 %
$gg \rightarrow b\bar{b}q\bar{q}(\gamma)$	0.0332(7)	0.03 %	0.124(3)	0.37 %
$q\bar{q} \rightarrow b\bar{b}gg(\gamma)$	0.0137(2)	0.01 %	0.094(2)	0.28 %
$q\bar{q} \rightarrow b\bar{b}q'\bar{q}'(\gamma)$	0.000080(3)	0.00007 %	0.00080(8)	0.002 %

Table 2: Partial contributions σ_i (σ_i^γ) in pb (fb) of the partonic sub-processes to the total cross section $\sigma = 103$ pb ($\sigma^\gamma = 33.5$ fb), corresponding to the background process $pp \rightarrow b\bar{b}jj(\gamma)$, for $m_H = 120$ GeV. Optimized kinematical cuts (set 1), as defined in Section 4, Eqs. (2) and (3), are implemented. The numbers in parenthesis correspond to the numerical errors on the last digit.

(σ_i/σ) cross sections for the QCD $b\bar{b}jj$ background corresponding to the different classes of partonic processes. An *optimized* set of kinematical cuts enhancing the S/B ratio [that will be discussed subsequently in Section 4, cf. Eqs. (2) and (3), set 1] is applied.

The main effective constraints for the $b\bar{b}jj$ channel, apart from the jet isolation, are a large invariant mass for the final jj system, namely $m_{jj} \gtrsim 800$ GeV, and the restriction on the $b\bar{b}$ invariant mass to be inside a window of $m_H(1 \pm 10\%)$. After applying these cuts, and considering the $m_H = 120$ GeV case, the total QCD $b\bar{b}jj$ cross section turns out to be $\sigma \simeq 103$ pb. Most of this cross section is due to the classes of diagrams involving gluons in the t -channel, as represented in Figure 3 (a–c). In particular, the latter give the main contributions to the cross sections for the subprocesses $gg \rightarrow b\bar{b} + gg$ and $gq \rightarrow b\bar{b} + gq$, $qq \rightarrow b\bar{b} + qq$, and $qq' \rightarrow b\bar{b} + qq'$, where $q' \neq q$. Subleading QCD contributions in Figure 3 (d–g) come from the fusion of initial partons in s -channel type diagrams, like in $gg \rightarrow b\bar{b} + q\bar{q}$, $q\bar{q} \rightarrow b\bar{b} + gg$, $q\bar{q} \rightarrow b\bar{b} + q'\bar{q}'$, with $q' \neq q$. Indeed, the s -channel propagator depletes these contributions with respect to diagrams (a–c), when a large invariant mass for the jj system is required.

Then, in the third and fourth columns of Table 2, we report the absolute (σ_i^γ) and fractional ($\sigma_i^\gamma/\sigma^\gamma$) production rates, respectively, for the different classes of diagrams contributing to the QCD $b\bar{b}\gamma jj$ background to the $H\gamma jj$ signal. The *optimized* set of

sub-processes	$\sigma_i^\gamma[\text{no } b \text{ rad}]$ (fb)	$\sigma_i^\gamma[\text{no } b \text{ rad}]/\sigma^\gamma[\text{no } b \text{ rad}]$
$gq \rightarrow b\bar{b}qq\gamma$	8.19(6)	47.8 %
$gg \rightarrow b\bar{b}gg\gamma$	0	0 %
$qq' \rightarrow b\bar{b}qq'\gamma$	2.80(2)	16.4 %
$qq \rightarrow b\bar{b}qq\gamma$	3.49(3)	20.4 %
$q\bar{q}' \rightarrow b\bar{b}q\bar{q}'\gamma$	1.57(2)	9.2 %
$q\bar{q} \rightarrow b\bar{b}q\bar{q}\gamma$	0.87(1)	5.1 %
$gg \rightarrow b\bar{b}q\bar{q}\gamma$	0.10(2)	0.6%
$q\bar{q} \rightarrow b\bar{b}gg\gamma$	0.096(2)	0.6 %
$q\bar{q} \rightarrow b\bar{b}q'q'\gamma$	0.0009(1)	0.005 %

Table 3: Partial contributions $\sigma_i^\gamma[\text{no } b \text{ rad}]$ (fb) of the partonic sub-processes to the total cross section $\sigma^\gamma[\text{no } b \text{ rad}] = 17.12(6)$ fb for to the background process $pp \rightarrow b\bar{b}jj\gamma$, when the photon radiation off b -quarks is switched off. The general setup is the same as in Table 2.

kinematical cuts (as in Section 4, Eqs. (2) and (3), set 1) is applied for $m_H = 120$ GeV. The corresponding total QCD $b\bar{b}\gamma jj$ cross section is $\sigma^\gamma \simeq 33$ fb.

One can see that the leading contribution to total cross sections is provided by the subprocess $gq \rightarrow b\bar{b}qq(\gamma)$, giving more than 50% in both the $b\bar{b}jj$ and $b\bar{b}\gamma jj$ cases. Next comes the $gg \rightarrow b\bar{b}gg(\gamma)$ channel, with contributions of roughly 24% and 12% to the σ and σ^γ total cross sections, respectively. The set of kinematical cuts imposed (in particular the large invariant mass of the jj system) requires quite large partonic energy fractions for the initial partons. This should suppress the relevance of gluon initiated channels with respect to the valence-quark initiated channel. Nevertheless, gluon initiated processes keep a leading role in contributing to the total background cross sections.

Now we can see why requiring a further central photon in VBF dramatically improves the detectability of the signal over the background. On the one hand, the requirement of a $p_T^\gamma \gtrsim 20$ GeV central photon in the Higgs boson VBF production decreases the production rates by a bit less than two orders of magnitude (*i.e.* accordingly to the naive QED scaling expectations), as we will see in Section 4 (cf. Tables 4 and 5). On the other hand, Table 2 shows that all the classes of partonic subprocesses that contribute by more than 1% to the irreducible-background cross sections are reduced by more than three orders of magnitude as an effect of requiring a further large p_T photon, giving an overall reduction factor in the background cross section of $\sigma^\gamma/\sigma \sim 1/3000$.

In particular, we can see that the cross section for the second leading source of background for the basic VBF, that is the $gg \rightarrow b\bar{b}gg$ channel, is reduced by more than a factor 1/6000 after the photon requirement, falling from ~ 25 pb down to ~ 4 fb for the $gg \rightarrow b\bar{b}gg\gamma$ channel. This is because gluons are neutral, and photons can only be emitted by the $b\bar{b}$ pair in this channel. Furthermore, the photon radiation by b quarks is also naturally suppressed by the down-quark electric charge.

The contribution arising from photon emission in the subprocesses $gq \rightarrow b\bar{b} + gq$, $qq' \rightarrow b\bar{b} + qq'$, and $qq \rightarrow b\bar{b} + qq$ might in principle be larger. Nevertheless, as shown in Table 2, it is reduced approximately by a factor 1/3300, 1/2000, and 1/1500 for the gq , qq' and qq initial states, respectively, which is still an order of magnitude below the naive expectation for QED radiative corrections.

This result can be explained in the following way. When the photon is forced to be emitted in the central rapidity region (here, we are requiring in particular for the photon pseudorapidity $|\eta_\gamma| \leq 2.5$), a destructive quantum interference arises between the photon emission off the initial quark radiating a gluon (or any other neutral vector boson) in the t channel, and the photon emission off the corresponding final quark. For instance, in the set of seven diagrams shown in Figure 4, the three subsets of diagrams [(a) + (b)], [(c) + (d)] and [(e)+(f)+(g)] are separately gauge invariant. One can check (for example in the eikonal approximation) that, inside the first two subsets, there is a strong destructive interference for photons emitted outside the typical radiation cone around the initial/final partons between the diagrams (a) – (b) and (c) – (d) in Figure 4. Since in t -channel diagrams final partons are mostly approximately collinear to the initial ones, requiring central $|\eta_\gamma|$'s indeed pushes photons outside the typical radiation cone.

In the third subset of diagrams, [(e)+(f)+(g)] in Figure 4, the photon is emitted from a b -quark line. For the b -quark emission, no destructive interference is expected, and its contribution turns out to be important, and even dominant, in many classes of diagrams in Table 2, even if it is controlled by the down-quark electric charge. This is shown in Table 3, where we compute again the entries of Table 2 for the radiative background $b\bar{b}\gamma jj$ after switching off the photon radiation from b -quarks in the complete matrix element. The background total cross section falls down to $\sigma^\gamma[\text{no } b \text{ rad}] = 17.3(3)$ fb in this case.

The destructive interference effect for central hard photons is even more manifest in Figure 5, where we plot the photon pseudorapidity distribution for the irreducible QCD background $pp \rightarrow b\bar{b}\gamma jj$ (solid curve). The effect of switching off the photon radiation from b quarks in the complete matrix element of the process is shown by the dashed line. The *optimized* kinematical cuts (set 1) defined in Section 4 [Eqs. (2)

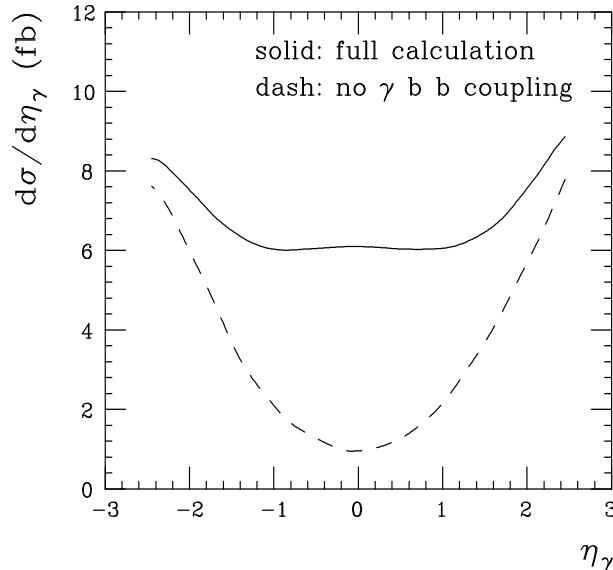


Figure 5: Effect of switching off the photon radiation from b quarks in the irreducible QCD background $pp \rightarrow b\bar{b}\gamma jj$ on the photon pseudorapidity distribution. The plot refers to the case $m_H = 120$ GeV. Solid line: full calculation for the *optimized* kinematical cuts (set 1) defined in Section 4, Eqs. (2) and (3). Dashed line: same as before, assuming vanishing b -quark coupling to photons.

and (3)] and $m_H = 120$ GeV are assumed. From the plot, one can see the relative weight of the photon radiation off initial/final (non b) quarks. The dashed line clearly shows a deep corresponding to the photon central rapidity region, and arising from the destructive interference between initial and final quarks radiation. This deep is only partially filled by the photon radiation off b quarks. We also checked that the same suppression at $\eta_\gamma \sim 0$ is observed for lower p_T^γ values, by relaxing the $p_T^{\gamma, cut}$ down to values as low as 5 GeV. In fact, the behaviour of a photon with a p_T as low as 20 GeV at LHC energies is already well described by the eikonal approximation.

For the signal case of the $H \gamma jj$ production (Figure 1), the above mechanism of destructive interferences affects only the diagrams involving the ZZ fusion. On the other hand, in the diagrams involving WW fusion (that are responsible for the dominant part of the basic VBF $H jj$ cross section) the charged currents in the $qq'W$ vertices change the electric charges of the in-out partons, and consequently the interference is now additive rather than destructive. Therefore, the cross section for $H \gamma jj$ is expected to follow the usual pattern of QED corrections as far as its WW fusion component is concerned. The relative contribution of the ZZ fusion will be instead remarkably smaller than in the case of the basic VBF $H jj$ process.

In order to prove this last statement, we selected, among all possible subprocesses

contributing to $pp \rightarrow H(\gamma)jj$, a first set of subprocesses (named N) mediated only by the ZZ fusion, namely $qq \rightarrow H(\gamma)qq$ [in particular, we summed up cross sections for $q = (u, d, s, c, \bar{u}, \bar{d}, \bar{s}, \bar{c})$], and a second set of subprocesses (named C) mediated only by the WW fusion [in this case, we summed up the 8 cross sections of the type $u\bar{c} \rightarrow H(\gamma)d\bar{s}$]. Calling $\sigma^{(N,C)}$ the cross sections for the two latter sets, we computed the following ratios among the radiative and the non-radiative processes at the LHC

$$\frac{\sigma^{(N)}(H\gamma jj)}{\sigma^{(N)}(Hjj)} = 0.0016, \quad \frac{\sigma^{(C)}(H\gamma jj)}{\sigma^{(C)}(Hjj)} = 0.013,$$

where we applied the cuts $p_T^\gamma \geq 20$ GeV, $|\eta_\gamma| \leq 2.5$, and $\Delta R_{j\gamma} \geq 0.7$, assuming $m_H = 120$ GeV. It is then clear that the radiation is suppressed in the presence of the HZZ vertex.

This property enhances the sensitivity of the $H\gamma jj$ cross section to the WWH coupling. Hence, a determination of the WWH coupling at the LHC could benefit also from a measurement of the $H\gamma jj$ cross section.

On the same basis, one can expect that the above destructive interference effect will also reduce the contribution from central photon radiation in the Higgs production through the $g^*g^* \rightarrow H$ process, giving also rise to $H\gamma jj$ final states. We verified that this is indeed the case. After applying the *basic* kinematical cuts in Eq. (2), Section 4, with $p_T^\gamma \geq 20$ GeV, we obtain a reduction factor of about $8 \cdot 10^{-4}$ for the $H\gamma jj$ cross section arising from the $g^*g^* \rightarrow H$ channel with respect to the corresponding Hjj cross section. In particular, the absolute value of the $H(\rightarrow b\bar{b})\gamma jj$ cross section (in the limit $m_t \rightarrow \infty$) turns out to be 0.21 fb, which makes the impact of the $g^*g^* \rightarrow H$ process on the present analysis negligible.

4 Cross sections for the signal versus the irreducible background

The numerical results presented in this section have been independently obtained by the Monte Carlo event generators ALPGEN [18], and MadEvent [19].

The signal is calculated in the narrow width approximation, *i.e.* we computed the exact lowest-order matrix element for the process $pp \rightarrow H\gamma jj$, and then let the Higgs boson decay into a $b\bar{b}$ pair according to its branching ratio and isotropic phase space. After the decay, cuts on the b -quark jets are implemented.

For the irreducible $pp \rightarrow b\bar{b}\gamma jj$ background, we computed all the matrix elements at $\mathcal{O}(\alpha_s^4\alpha)$, neglecting $\mathcal{O}(\alpha_s^2\alpha^3)$, $\mathcal{O}(\alpha_s\alpha^4)$ and $\mathcal{O}(\alpha^5)$ contributions and their interference with the $\mathcal{O}(\alpha_s^4\alpha)$ contribution. We checked that this has no numerical impact

on the results.

The present study is limited at the parton level, apart from some preliminary analysis of parton-shower effects presented in Section 6. A more complete simulation, that takes into account showering, hadronization and detector simulation, even if crucial for the assessment of the potential of this channel, is beyond the scope of the present paper.

As PDF's, we use the parametric form of CTEQ5L [20], and the factorization/re-normalization scales are fixed at $\mu_F^2 = \mu_R^2 = \sum E_t^2$ and $\mu_F^2 = \mu_R^2 = m_H^2 + \sum E_t^2$ for the backgrounds and signal, respectively (E_t is the transverse energy of any QCD parton). The three Higgs-mass cases 120, 130 and 140 GeV are analysed.

We start by the definition of two *basic* event selections (sets 1 and 2) that differ only by the threshold on the photon transverse momentum p_T^γ :

$$\begin{aligned}
& p_T^j \geq 30 \text{ GeV}, \quad p_T^b \geq 30 \text{ GeV}, \quad \Delta R_{ik} \geq 0.7, \\
& |\eta_\gamma| \leq 2.5, \quad |\eta_b| \leq 2.5, \quad |\eta_j| \leq 5, \\
& m_{jj} > 400 \text{ GeV}, \quad m_H(1 - 10\%) \leq m_{b\bar{b}} \leq m_H(1 + 10\%), \\
& 1) \quad p_T^\gamma \geq 20 \text{ GeV}, \\
& 2) \quad p_T^\gamma \geq 30 \text{ GeV},
\end{aligned} \tag{2}$$

where ik is any pair of partons in the final state, including the photon, and $\Delta R_{ik} = \sqrt{\Delta^2 \eta_{ik} + \Delta^2 \phi_{ik}}$, with η the pseudorapidity and ϕ the azimuthal angle. Note that the $m_{b\bar{b}}$ cut is only effective on the continuous $m_{b\bar{b}}$ backgrounds. On the other hand, the finite $m_{b\bar{b}}$ resolution will also affect the following analysis of the expected signal event rate that, in the present m_H range, has a natural width for the $m_{b\bar{b}}$ distribution much smaller than the $m_{b\bar{b}}$ resolution. The cross sections for the above *basic* event selections are reported in Table 4. Cross sections for the signal and irreducible background for the VBF Hjj process (named from now on “signal without photon” and “background without photon”, respectively) are also shown, assuming the same kinematical cuts.

For comparison, requiring the leptonic (both μ^\pm and e^\pm) signature for the W in the $HWjj$ process [16], by applying the same event selection of Eq. (2) (with the constraints on the photon applied to the charged lepton, and $p_T^\ell > 20$ GeV), we find a $H(\rightarrow b\bar{b})\ell\nu jj$ cross section of 2.1 fb, for $m_H = 120$ GeV. From Table 4, one then obtains that the rate for the $H\gamma jj$ signal is about 4.4 times the $H\ell\nu jj$ rate, for $m_H = 120$ GeV.

With the same event selection of Eq. (2) (Set 1), we also computed the cross section for the $b\bar{b}\gamma jj$ final states mediated by an on-shell Z decay $Z \rightarrow b\bar{b}$. For the purely electroweak process, we obtained a cross section of 10 fb, while, for the QCD mediated channel, we obtained a cross section of 26 fb. As we previously noted, we

	$p_T^{\gamma, cut}$	$m_H = 120$ GeV	$m_H = 130$ GeV	$m_H = 140$ GeV
$\sigma[H(\rightarrow b\bar{b})\gamma jj]$	20 GeV	9.3(1) fb	7.4(1) fb	4.74(7) fb
	30 GeV	6.54(7) fb	5.2(1) fb	3.31(3) fb
$\sigma[b\bar{b}\gamma jj]$	20 GeV	406(2) fb	405(4) fb	389(1) fb
	30 GeV	260.5(7) fb	257.9(6) fb	251.8(7) fb
$\sigma[H(\rightarrow b\bar{b})jj]$		727(2) fb	566(2) fb	363(1) fb
$\sigma[b\bar{b}jj]$		593.7(5) pb	550.5(5) pb	505.6(4) pb

Table 4: Cross sections for the signal and the irreducible background for the *basic* event selections in Eq. (2). Higgs production cross sections include the Higgs branching ratios to $b\bar{b}$. The signal and irreducible background production rates for the VBF process without photon are also shown.

do not expect any contamination from this background, since its typical $b\bar{b}$ invariant mass is well below the Higgs boson mass range considered here, for the foreseen experimental resolution on $m_{b\bar{b}}$.

Before comparing the signal and the background for the $H\gamma jj$ process, we tried to optimize our event selection in Eq. (2). Indeed, the signal detectability can be further improved by imposing *optimized* cuts, that can be deduced by looking at the following kinematical distributions (Figures 6, 7):

$$\frac{d\sigma}{dm_{jj}}, \quad \frac{d\sigma}{dp_T^{j1}}, \quad \frac{d\sigma}{dp_T^{b1}}, \quad \frac{d\sigma}{dm_{\gamma H}}, \quad \frac{d\sigma}{|\Delta\eta_{jj}|},$$

where $j1$ and $b1$ denote the leading p_T light jet and b -jet, respectively, and $m_{\gamma H}$ is the invariant mass of the $\gamma b\bar{b}$ system. The most effective cut in reducing the background with respect to the signal is related to the $d\sigma/dm_{jj}$ distribution in Figure 6, as already noted in [10] for the case without photon.

An interesting general feature is that the shapes of the distributions with and without the photon are similar, as shown by the closeness of the solid and dot-dashed lines on the one side, and of the dashed and dotted lines on the other side, in Figures 6 and 7. This shows that the effect of QED radiation is dominated by the factorized eikonal approximation, since most of the p_T^{γ} values considered are soft with respect to the energy scale of the process. On the other hand, some differences between the radiative and the non-radiative processes are present, that can help significantly in improving the S/B ratio.

Indeed, the request of a further central photon tends to enhance the characteristic kinematical features of a typical VBF event. First of all, the jj invariant mass distribution is flatter for the radiative signal than for the non radiative case (see solid and

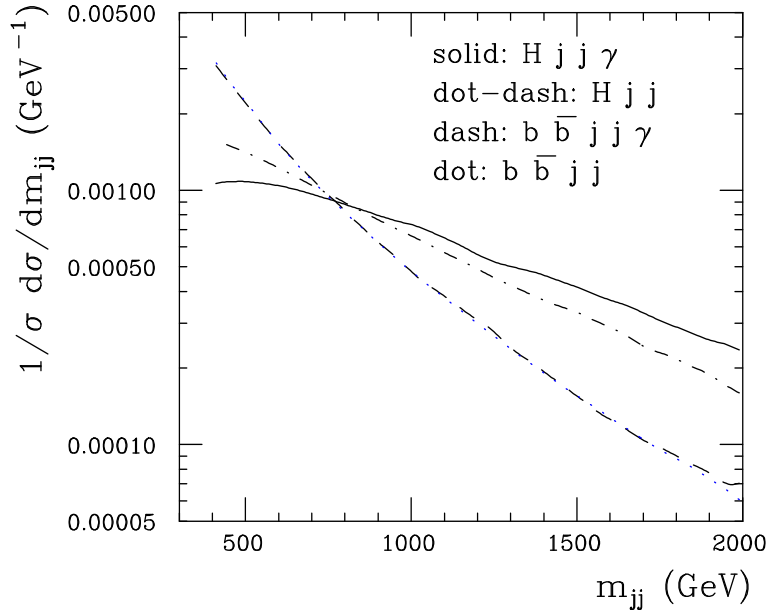


Figure 6: The two forward-jet invariant mass distribution (critical to increase S/B). Solid line: signal with photon. Dashed line: irreducible background with photon. Dot-dashed line: signal without photon. Dotted line: irreducible background without photon. Cuts in Eq. (2) are applied, and $m_H = 120$ GeV.

dot-dashed lines in Figure 6), while the corresponding backgrounds are almost superimposed. Then, increasing the lower m_{jj} cut does not imply a dramatic reduction of the signal cross section, while it gains a substantial decrease of the background. Second, by adding the photon, the distribution $d\sigma/d|\Delta\eta_{jj}|$ is slightly shifted toward larger $|\Delta\eta_{jj}|$ values for the signal, while it moves in the opposite direction for the background. This feature makes a cut on the pseudorapidity separation between the tagging jets even more effective than in the case of the VBF $H jj$ typical event [10].

By studying the variation of the significance S/\sqrt{B} as a function of the cuts on the distributions [†], we found an *optimized* event selection where, in addition to the *basic* cuts, we impose the following cuts [‡]:

$$\begin{aligned}
 m_{jj} \geq 800 \text{ GeV}, \quad p_T^{j1} \geq 60 \text{ GeV}, \quad p_T^{b1} \geq 60 \text{ GeV}, \\
 |\Delta\eta_{jj}| > 4, \quad m_{\gamma H} \geq 160 \text{ GeV}, \quad \Delta R_{\gamma b/\gamma j} \geq 1.2.
 \end{aligned}
 \tag{3}$$

With the above additional requirements, we find the cross sections reported in Table 5,

[†]This was performed for $m_H = 120$ GeV. For higher Higgs masses the constraints in Eq. (3) (especially the one on $m_{\gamma H}$) could be further tuned.

[‡]There are few more distributions which show differences between signal and backgrounds. However these are not exploited here, since, at the parton level of the present analysis, they lead to an improvement in S/B , but not in S/\sqrt{B} .

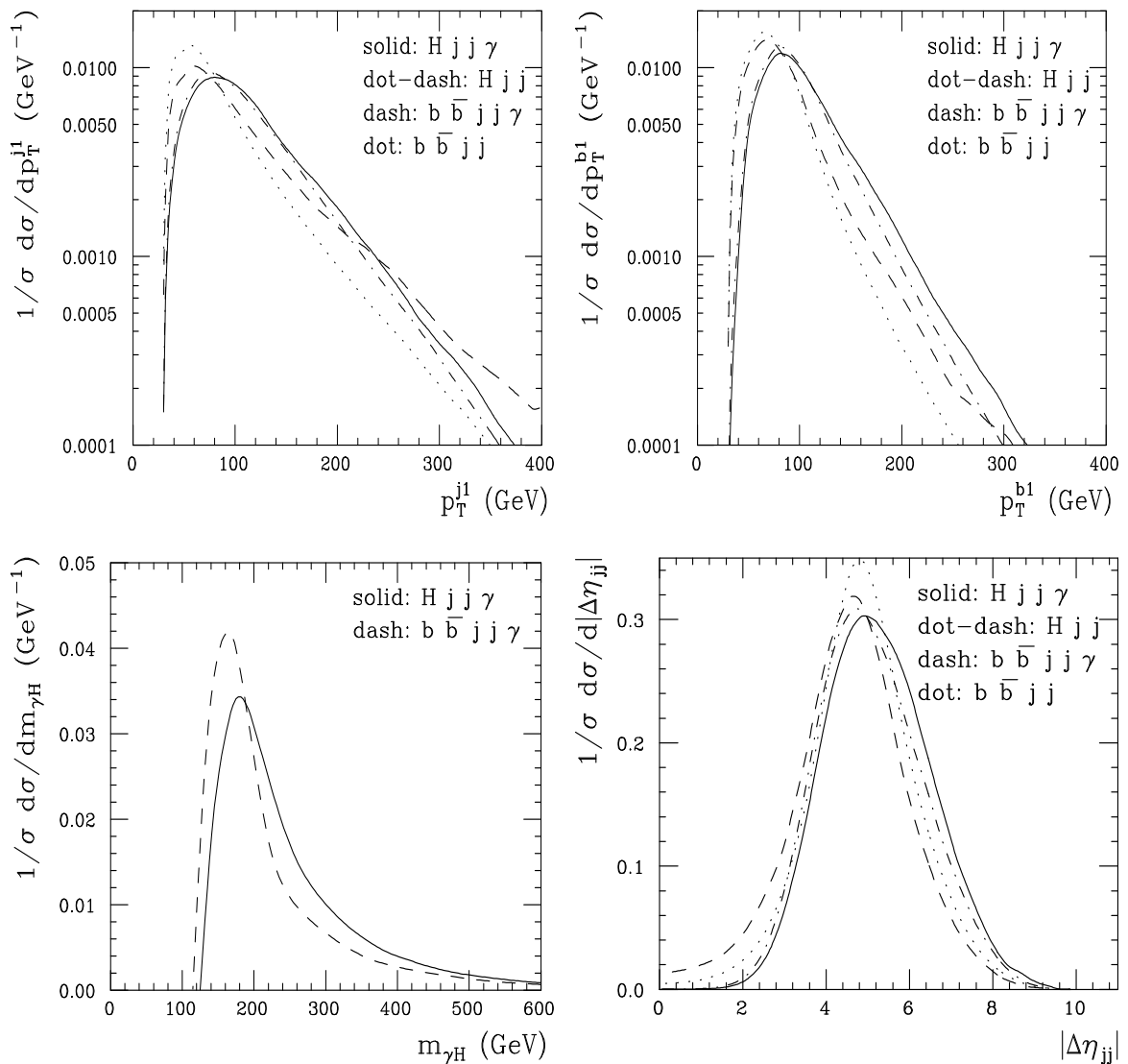


Figure 7: Four further different distributions used to optimize cuts to improve the S/B ratio. Upper left panel: leading light jet p_T distribution. Upper right panel: leading b jet p_T distribution. Lower left panel: invariant mass distribution for the Higgs boson-plus-photon system. Lower right panel: distribution for the difference in pseudorapidity of the two light jets. Solid line: signal with photon. Dashed line: irreducible background with photon. Dot-dashed line: signal without photon. Dotted line: irreducible background without photon. Cuts in Eq. (2) are applied, and $m_H = 120$ GeV.

	$p_T^{\gamma, cut}$	$m_H = 120$ GeV	$m_H = 130$ GeV	$m_H = 140$ GeV
$\sigma[H(\rightarrow b\bar{b})\gamma jj]$	20 GeV	3.59(7) fb	2.92(4) fb	1.98(3) fb
	30 GeV	2.62(3) fb	2.10(2) fb	1.50(3) fb
$\sigma[b\bar{b}\gamma jj]$	20 GeV	33.5(1) fb	37.8(2) fb	40.2(1) fb
	30 GeV	25.7(1) fb	27.7(1) fb	28.9(2) fb
$\sigma[H(\rightarrow b\bar{b})jj]$		320(1) fb	254.8(6) fb	167.7(3) fb
$\sigma[b\bar{b}jj]$		103.4(2) pb	102.0(2) pb	98.4(2) pb

Table 5: Cross sections for the signal and the irreducible background for the *optimized* event selections of Eq. (3), added to the *basic* selection in Eq. (2). Higgs production cross sections include the Higgs branching ratios to $b\bar{b}$. The signal and irreducible background production rates for the basic VBF process are also shown.

where also the signal and irreducible background production rates for the VBF process without photon are shown.

A comment on the sensitivity to the choice of the factorization/renormalization scale is in order. While the signal is mediated by electroweak gauge bosons, and thus depends on α_s only through the PDF's, the background contains four powers of α_s and thus it is expected to be more sensitive to scale variations. We expect our scale choice $\mu_F^2 = \mu_R^2 = \sum E_t^2$ provides a conservative estimate of the background cross section, given the large \hat{s} values of the elementary processes involved (arising from the large mass threshold for the pair of forward jets). We have, however, evaluated the impact of a variation of μ_F^2 and μ_R^2 by a factor of two, obtaining a variation of about 25-30% in the cross section. This translates into an uncertainty of the order of 10-15% on the statistical significances studied in the following, thus being of moderate impact.

As anticipated in Section 3, one can see in Table 5 that the requirement of the extra central photon with $p_T^\gamma \gtrsim 20$ GeV in the final state involves a reduction factor of order 100 for the signal rate with respect to the final state without photon, according to the expectations of the $\mathcal{O}(\alpha)$ QED naive scaling. On the other hand, the radiative background is suppressed by a factor of about 3000 with respect to the case of no photon radiation. As also discussed in Section 3, this effect can be understood as due to the quantum destructive interference between the photon emission from the initial quark radiating a gluon in the t channel and the photon emission from the corresponding final quark. Such an effect makes the process $b\bar{b}\gamma jj$ competitive on the statistical significance with the process $b\bar{b}jj$ studied in [10].

Furthermore, the presence of an additional photon can improve the experimental

	$p_T^{\gamma,cut}$	$m_H = 120$ GeV	$m_H = 130$ GeV	$m_H = 140$ GeV
$S/\sqrt{B} _{H\gamma jj}$	20 GeV	2.6	2.0	1.3
$S/\sqrt{B} _{H\gamma jj}$	30 GeV	2.2	1.7	1.2
$S/\sqrt{B} _{Hjj}$		3.5	2.8	1.9

Table 6: Statistical significances with the event selection of Eq. (2) and (3), with an integrated luminosity of 100 fb^{-1} . The value $\epsilon_b = 60\%$ for the b -tagging efficiency and a Higgs boson event reduction by $\epsilon_{b\bar{b}} \simeq 70\%$, due to the finite ($\pm 10\%$) $b\bar{b}$ mass resolution, have been assumed. Jet-tagging efficiency and photon-identification efficiency are set to 100%. Only the irreducible background is included in this analysis.

triggering efficiencies, provided a good rejection of jets against photons is available [21, 22]. Triggering on an inclusive photon with a p_T threshold of 22 GeV gives a Level-1 trigger rate of about 4.2 kHz in the CMS detector with an instantaneous luminosity $\mathcal{L} = 2 \times 10^{33} \text{ cm}^{-2} \text{ s}^{-1}$ [23, 24]. Similar performances are expected for the ATLAS detector [25]. This rate might be further reduced with a High Level Trigger (HLT) based on the combined presence of photon plus heavy flavours or photon plus forward tagging jets. Such HLT studies have not yet been done.

The effect of the inclusion of optimized cuts as in Eq. (3) is to reduce the signal cross sections by about a factor of two, while the background gets scaled by about an order of magnitude, allowing to reach a S/B ratio for cross sections larger than $1/10$ at $m_H \simeq 120$ GeV, for both values of the $p_T^{\gamma,cut}$. The corresponding ratio for the case without photon is about $1/300$. At $m_H \simeq 140$ GeV, both the S/B ratios fall down by about a factor two.

In order to evaluate the expected statistical significance of the signal, we assumed a b -tagging efficiency $\epsilon_b = 60\%$, and a reduction of the *signal* number of events by 70% in the window $m_H(1 \pm 10\%)$, due to the finite $b\bar{b}$ mass resolution, that broadens the narrow Higgs decay $b\bar{b}$ distribution. For an integrated luminosity of 100 fb^{-1} , we get a statistical significance $S/\sqrt{B}|_{H\gamma jj} \simeq 3$, at low m_H and $p_T^{\gamma,cut}$ values. At $m_H \simeq 140$ GeV and $p_T^{\gamma,cut} \simeq 30$ GeV, it degrades down to about 1.3, mainly due to the falling branching ratio for $H \rightarrow b\bar{b}$. This is to be compared with $S/\sqrt{B}|_{Hjj}$ that ranges from 3.5 down to about 2. A summary of the statistical significances, including only the irreducible background, with an integrated luminosity of 100 fb^{-1} is given in Table 6.

5 Reducible backgrounds

A complete analysis of the reducible backgrounds to the $H\gamma jj$ signal is beyond the scope of our study. For instance, the potential dangerous contamination coming from π^0 decays into photons can only be studied with a simulation including showering, hadronization and detector simulation, and is left to a further investigation. However, in order to have a sensible estimate of the achievable S/B ratio and statistical significance at parton level, we computed with ALPGEN the cross sections, assuming $m_H = 120$ GeV and with the optimized event selection of Eq. (2) and (3), for three main potentially dangerous processes [§]:

- $pp \rightarrow \gamma + 4$ jets, where two among the light jets are fake tagged as b -jets;
- $pp \rightarrow b\bar{b} + 3$ jets, where one of the light jets is misidentified as a photon;
- $pp \rightarrow 5$ jets, where one of the light jets is misidentified as a photon, and two light jets are fake tagged as b -jets.

With more than two light jets in the final state, the selection criteria need to be specified, in order to avoid ambiguities. Even if some algorithm able to mimic a realistic analysis should be implemented, we adopt a very simple one, which however should give us a sound estimate of the cross sections. At first, we look for the pair of light jets with the largest invariant mass, and identify the latter as the tagging jets. For the channel $\gamma + 4$ jets, this is enough to guarantee also a unique assignment for the fake b -jets. In the case of the $b\bar{b} + 3$ jets final state, once we have specified the tagging jets, the remaining light jet is the one misidentified as the photon. An additional specification is required for the 5 jet channel. After the tagging jet selection, we choose the photon at random among the remaining three light jets. Then, the remaining two jets are the fake b -tagged jets. With the above specifications of the event selection, keeping the same setup for the energy scales and PDF's as in the previous Section, we obtain the cross sections quoted in Table 7. The quoted cross sections should then be multiplied by the appropriate efficiencies: ϵ_{fake}^2 for $pp \rightarrow \gamma + 4$ jets, $\epsilon_b^2 \epsilon_{\gamma j}$ for $pp \rightarrow b\bar{b} + 3$ jets and $3 \epsilon_{\text{fake}}^2 \epsilon_{\gamma j}$ for $pp \rightarrow 5$ jets, where ϵ_{fake} is the efficiency of mistagging a light jet as a b -jet, and $\epsilon_{\gamma j}$ is the rejection factor of a jet against a photon. Adopting the same efficiencies as in Table 6, and assuming $\epsilon_{\text{fake}} = 1\%$ and $\epsilon_{\gamma j} = 1/5000$ [¶], we obtain the event numbers for signal and backgrounds shown in Table 8, assuming $m_H = 120$ GeV and an integrated luminosity of 100 fb^{-1} . As

[§] We estimated that the process $pp \rightarrow c\bar{c}\gamma jj$, where the c quarks are both mistagged as b quarks, (assuming $\epsilon_c = 10\%$) can be safely neglected.

[¶]This is the value quoted in [21], see also [22].

	$p_T^\gamma \geq 20$ GeV	$p_T^\gamma \geq 30$ GeV
$\sigma(pp \rightarrow \gamma + 4j)$	2.27(2) pb	1.72(4) pb
$\sigma(pp \rightarrow b\bar{b} + 3j)$	61.1(3) pb	45.1(2) pb
$\sigma(pp \rightarrow 5j)$	2.40(1) nb	1.83(1) nb

Table 7: Cross sections for reducible background channels, for the optimized event selections of Eq. (2) and (3), applied as explained in the text. The value $m_H = 120$ GeV is assumed.

	$p_T^\gamma \geq 20$ GeV	$p_T^\gamma \geq 30$ GeV
$pp \rightarrow \gamma H(\rightarrow b\bar{b}) + 2j$	90	66
$pp \rightarrow \gamma b\bar{b} + 2j$	1206	925
$pp \rightarrow \gamma + 4j$	23	17
$pp \rightarrow b\bar{b} + 3j$	440	324
$pp \rightarrow 5j$	14	11
S/\sqrt{B}	2.2	1.8

Table 8: Event numbers for signal, irreducible and reducible backgrounds, for the case $m_H = 120$ GeV, with an integrated luminosity of 100 fb^{-1} . The efficiencies are described in the text. The last line shows the statistical significance including all the background channels.

can be seen in the last line of Table 8, by including also the reducible backgrounds, the statistical significance decreases by about 14(12)% for $p_T^{\gamma, cut} = 20(30)$ GeV) with respect to Table 6, where only the irreducible background has been considered. The most dangerous contribution to reducible backgrounds comes from $pp \rightarrow b\bar{b} + 3j$.

A possible way of increasing the number of signal events is to require at least one b -tag instead of two. In fact, with $\epsilon_b = 60\%$, the effective tagging efficiency becomes $2\epsilon_b(1 - \epsilon_b) + \epsilon_b^2 = 0.84$, instead of $\epsilon_b^2 = 0.36$. Then, considering only the irreducible background, the S/B ratio remains unchanged but the significance increases by a factor of about 1.5. We have also performed a preliminary analysis of event numbers assuming single b -tagging. Omitting potentially large reducible backgrounds, such as multi-jet processes with one heavy quark and a mistagged jet, we found a significance slightly below the one obtained in the two b -tag case. This conclusion, however, relies strongly on the assumed fake tag probabilities, which can be estimated only with a full detector simulation. It could therefore be worthwhile to investigate also this possibility.

6 Parton-shower effects and central jet veto

A feature of the signal is that to leading order no colour is exchanged between the up and down fermionic lines of Figure 1, since $pp \rightarrow H\gamma jj$ is an electroweak mediated process [26]. Thus the typical scale for QCD radiation is p_T^j . On the contrary, the diagrams of the background processes are characterized by the presence of t -channel virtual gluons (cf. Figure 4). Thus the typical scale for QCD radiation is of the order of 1 TeV ($m_{jj} + m_H$). On these grounds, we can expect that higher-order QCD radiation will be much more relevant for the background than for the signal. The fairly different radiation pattern can be exploited to further enhance the S/B ratio, as suggested in [26]. We investigated qualitatively these features by simulating higher-order QCD radiation with the HERWIG parton shower [27] on top of the partonic unweighted events, generated with ALPGEN with the optimized event selection of Eqs. (2) and (3), set 1. This is not a completely consistent approach, since one is sensitive to the partonic event selection, which has no physical meaning. A more solid study could be done by using a consistent matching procedure between parton shower and multi-parton matrix elements [28], which amounts to merging together event samples originating from different partonic multiplicities. We have however verified that, restricting our analysis to a sample with cuts tighter than parton level cuts, results are essentially unchanged, and we are therefore confident that a more refined study would lead to not too different results.

Since the aim of this section is simply to give a qualitative estimate of the effects of a realistic event simulation, we will restrict ourselves to the naive procedure of showering the events with partonic cuts corresponding to the final event selection. The value $m_H = 120$ GeV is considered. Jets are defined via a cone algorithm using the routine GETJET [29], which uses a simplified version of the UA1 jet algorithm, with parameters given by

$$p_T^j > 20, \text{ GeV}, \quad |\eta_j| < 5, \quad R = 0.7, \quad (4)$$

where R is the jet cone radius. The b -tagged jets are defined as the ones containing the original b quarks.

Given the presence of extra QCD radiation, the identification of light tagging jets, among the remaining ones, is not uniquely defined. We explored two different algorithms: as a first choice, the tagging jets are identified by the highest and second highest p_T jets (referred to as algorithm $a1$); an alternative is to identify the tagging jets as the pair of jets with the highest invariant mass (algorithm $a2$). For both event selections we require $p_T^{j1} \geq 60$ GeV and $p_T^{j2} \geq 30$ GeV. The results are shown in Figure 8. In particular, the panels in the first row show the invariant mass distribution of signal and background (solid and dashed histogram, respectively), for tagging jet identifications $a1$ and $a2$. While the signal is practically insensitive to the choice between the algorithm $a1$ and $a2$, the background shows a large difference. With the choice $a1$, a large fraction of events gives rise to a sort of peak at low invariant masses. Using this choice to select the tagging jets, while a cut on the invariant mass of the tagging jets $m_{jj} \geq 800$ GeV, applied after the shower, would reduce the signal only by about 7%, the same cut would reduce the background by a factor of about two. We expect the peak at low invariant masses to be due to the identification of tagging jets with jets originated from the shower and not containing the original hard partons. This interpretation is confirmed by the panels in the second row, which shows the $|\Delta\eta_{jj}|$ distributions for signal and background (solid and dashed histogram, respectively). On the left the eta separation between the tagging jets, defined according to algorithm $a1$, is shown. While for almost all signal events one has $|\Delta\eta_{jj}| \geq 4$, a consistent portion of background events displays a smaller rapidity separation. In these events, at least one of the tagging jets originates from higher order parton shower emission. By looking for the pair of jets satisfying the tagging requirement $p_T^{j1} \geq 60$ GeV and $p_T^{j2} \geq 30$ GeV, with the additional constraint of maximum pseudorapidity separation, the correspondence between tagging jets and parton level jets is restored, as shown in the panel on the right.

The lower panels of Figure 8 give an estimate of the jet multiplicity (left) in signal (solid line) and background (dashed line), after $a1$ event selection has been

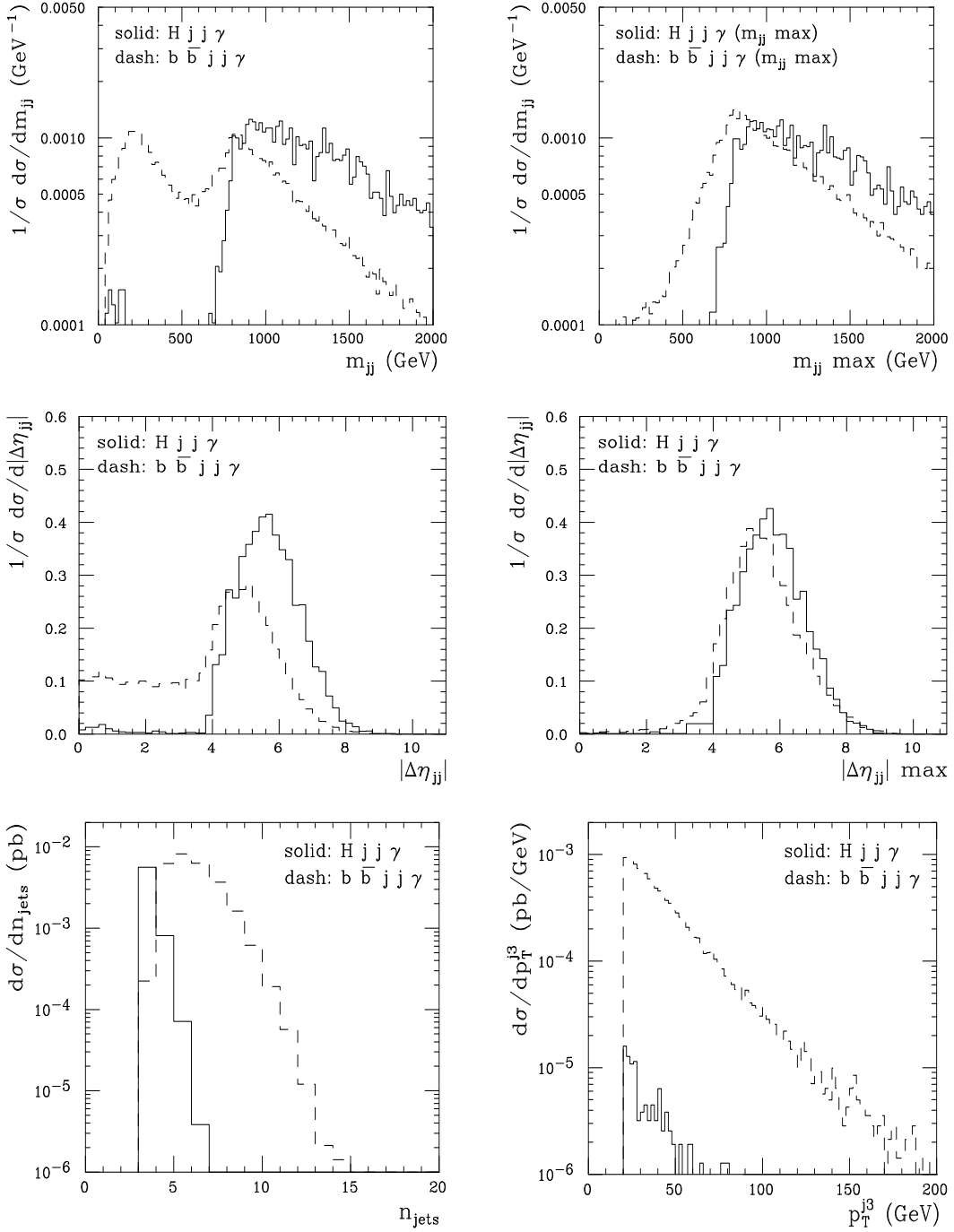


Figure 8: First row: m_{jj} distribution of the highest and second highest p_T jets after shower for signal and background (left), and maximum m_{jj} distribution among all possible jet pairs satisfying the tagging requirements (right). Second row: $|\Delta\eta_{jj}|$ distribution for the highest and second highest p_T jets after shower (left), and maximum pseudorapidity separation between jets satisfying the tagging p_T thresholds (right). Third row: jet multiplicity distribution for signal and background (left); p_T distribution of the third highest p_T jet (right).

applied with the additional cut on m_{jj} at the jet level. In this case we increased the threshold up to 1000 GeV, in order to minimize possible dependence on parton level cuts. While in the former case the jet multiplicity is sharply peaked at the value of four, in the latter case a much broader spectrum is present. On the right panel the p_T distribution of an additional p_T ordered jet with $p_T \geq 20$ GeV and pseudorapidity between the tagging jet η 's is shown. If one imposes a further cut $m_{jj} \geq 1000$ GeV (the result is only slightly changed if $m_{jj} \geq 800$ GeV is used), a fraction of the order of 60%(50%) of the background events contains at least an extra jet with $p_T \geq 20(30)$ GeV, while only a small fraction (of the order of 2%) of the signal events contain such additional radiation. Thus a veto on additional jet activity in the central rapidity region, proposed for heavy and light Higgs searches in [30], could be very effective in suppressing the background more than the signal.

In principle, an additional handle to further suppress the background is given by the photon isolation criteria. For instance, we checked that, with our simplified calorimeter, a good choice could be to require no charged tracks with $p_T \geq 1$ GeV within a cone $\Delta R \simeq 0.2$ around the photon. For a quantitative statement, a full detector simulation is required. However, we expect that, for the present event selection, this kind of photon isolation criteria would actually lead to a small improvement in significance, rather than lowering the significance, as one would naively expect.

Even if a more refined analysis will be necessary for quantitative statements, we expect that the background events could be lowered by a factor of about four with respect to the partonic estimates of previous sections, once showering effects are included in the analysis and a central jet veto strategy is adopted. On the other hand, the signal seems to be almost insensitive to shower and central jet veto effects. This would lead to an improvement of about a factor of two in the signal significance.

7 Conclusions

In this paper, we studied the detectability of the Higgs boson production signal, when the Higgs boson is accompanied by a high- p_T central photon and two forward jets at the LHC. The Higgs boson decay into a $b\bar{b}$ pair is considered. We analyzed the signal, the irreducible QCD background, and main reducible backgrounds at the parton level. The presence of a photon in the final state can improve the triggering efficiencies with respect to the basic VBF Higgs production without a photon. Moreover, we find that the requirement of a central photon in addition to the typical VBF final-state topology significantly suppresses the irreducible QCD background. In particular, the latter has rates that are lower than the expectations of the $\mathcal{O}(\alpha)$ QED naive scaling by more

than an order of magnitude. We discussed thoroughly the dynamical effects that are responsible for this reduction. As a consequence, after optimizing kinematical cuts, we obtain a statistical significance S/\sqrt{B} for the $H(\rightarrow b\bar{b})\gamma jj$ channel that goes from around 3, if $m_H \simeq 120$ GeV, down to about 1.5, if $m_H \simeq 140$ GeV, for an integrated luminosity of 100 fb^{-1} . These significances are not far from the corresponding values for the basic $H(\rightarrow b\bar{b})jj$ process without a photon. The latter estimates are based on the irreducible QCD background. The impact of including a few main reducible backgrounds has also been studied, and found to be moderate.

A preliminary analysis of parton-shower effects points to a further differentiation between the signal and background final-state topology and composition. In particular, a preliminary analysis of showering and central jet veto effects points to an improvement of S/\sqrt{B} by a factor of two.

The same dynamical effects that are responsible for the irreducible background suppression also remarkably curb the relative contribution of the $ZZ \rightarrow H$ boson fusion diagrams with respect to the $WW \rightarrow H$ ones in the process $pp \rightarrow H(\rightarrow b\bar{b})\gamma jj$. As a consequence, we think that the study of the $H(\rightarrow b\bar{b})\gamma jj$ signal at the LHC could have a role in the determination of both the Hbb and HWW couplings. Further studies, including complete showering, hadronization, and detector simulations, that are beyond the scopes of the present paper, will be needed to establish the actual potential of the process $H(\rightarrow b\bar{b})\gamma jj$ in this field.

Acknowledgments

We wish to thank Anindya Datta for his contribution during the early stages of this work, and Paul Hoyer and Antonello Polosa for useful discussions. We thank Alexandre Nikitenko and Antonio Sidoti for many useful discussions on trigger issues. E.G., M.M. and F.P. also wish to thank the CERN Theory Unit for partial support and hospitality. B.M.'s and R.P.'s research was partially supported by the RTN European Programme MRTN-CT-2006-035505 (HEPTOOLS, Tools and Precision Calculations for Physics Discoveries at Colliders). B.M.'s research was also partially supported by the RTN European Programme MRTN-CT-2004-503369 (Quest for Unification). The work of E.G. was supported by the Academy of Finland (project number 104368). The research of R.P. was supported in part by MIUR under contract 2006020509_004.

References

- [1] The LEP Collaborations, ALEPH, DELPHI, L3, OPAL and the LEP Electroweak Working Group, arXiv:hep-ex/0612034; G. Abbiendi et al., Phys. Lett. B **565** (2003) 61 [arXiv:hep-ex/0306033].
- [2] S. Dawson, J.F. Gunion, H.E. Haber, and G. Kane, The Higgs Hunter's Guide (1989).
- [3] R. F. Dashen and H. Neuberger, Phys. Rev. D **66** (2002) 010001.
- [4] M. Luscher and P. Weisz, Phys. Lett. B **212** (1988) 472.
- [5] S. Heinemeyer, W. Hollik and G. Weiglein, JHEP **0006** (2000) 009 [arXiv:hep-ph/9909540], and references therein.
- [6] The Higgs Working Group Collaboration (K.A. Assamagan et al.), Les Houches 2003, Physics at TeV colliders, 1-169. arXiv:hep-ph/0406152. For a recent review on Higgs physics, see also A. Djouadi, arXiv:hep-ph/0503172, arXiv:hep-ph/0503173.
- [7] D. L. Rainwater and D. Zeppenfeld, JHEP **9712** (1997) 005 [arXiv:hep-ph/9712271].
- [8] D. L. Rainwater, D. Zeppenfeld and K. Hagiwara, Phys. Rev. D **59** (1999) 014037 [arXiv:hep-ph/9808468]; T. Plehn, D. L. Rainwater and D. Zeppenfeld, Phys. Rev. D **61** (2000) 093005 [arXiv:hep-ph/9911385].
- [9] M. Duhrssen, S. Heinemeyer, H. Logan, D. Rainwater, G. Weiglein and D. Zeppenfeld, Phys. Rev. D **70** (2004) 113009 [arXiv:hep-ph/0406323].
- [10] M.L. Mangano, M. Moretti, F. Piccinini, R. Pittau, and A.D. Polosa, Phys. Lett. **B556** (2003) 50 [arXiv:hep-ph/0210261].
- [11] E. Richter-Was and M. Sapinski, Acta Phys. Polon. **B30** (1999) 1001.
- [12] V. Drollinger, T. Muller, and D. Denegri, CERN-CMS-NOTE-2001-054 [arXiv:hep-ph/0111312].
- [13] S. Cucciarelli *et al.*, CERN-CMS-NOTE-2006-119.
- [14] V. Del Duca, W. Kilgore, C. Oleari, C. Schmidt and D. Zeppenfeld, Phys. Rev. Lett. **87** (2001) 122001 [arXiv:hep-ph/0105129]; Nucl. Phys. B **616** (2001) 367 [arXiv:hep-ph/0108030].

- [15] A. Abbasabadi, D. Bowser-Chao, D. A. Dicus, W. W. Repko, Phys. Rev. **D58** (1998) 057301 [arXiv:hep-ph/9706335].
- [16] D. L. Rainwater, Phys. Lett. B **503** (2001) 320 [arXiv:hep-ph/0004119].
- [17] A. Djouadi, J. Kalinowski and M. Spira, Comput. Phys. Commun. **108** (1998) 56 [arXiv:hep-ph/9704448].
- [18] M. L. Mangano, M. Moretti, F. Piccinini, R. Pittau and A. D. Polosa, JHEP **0307** (2003) 001 [arXiv:hep-ph/0206293].
- [19] F. Maltoni and T. Stelzer, JHEP **0302** (2003) 027 [arXiv:hep-ph/0208156].
- [20] H. L. Lai *et al.* [CTEQ Collaboration], Eur. Phys. J. C **12** (2000) 375 [arXiv:hep-ph/9903282].
- [21] M. Escalier, F. Derue, L. Fayard, M. Kado, B. Laforge, C. Reifen and G. Unal, ATL-PHYS-PUB-2005-018.
- [22] M. Pieri, K. Armourt and J.G. Branson, CERN-CMS-Note-2006-007.
- [23] CMS Collaboration, Physics Technical Design Report, Volume II: Physics Performance, CERN/LHCC 2006-021, CMS TDR 8.2 (2006).
- [24] G.M. Dallavalle and A. Sidoti, Internal Note ATL-COM-DAQ-2007-003.
- [25] Atlas Collaboration, “Detector and physics performance Technical Design Report”, CERN/LHCC/99-15.
- [26] Y. L. Dokshitzer, S. I. Troian and V. A. Khoze, Sov. J. Nucl. Phys. **46** (1987) 712 [Yad. Fiz. **46** (1987) 1220]; Y. L. Dokshitzer, V. A. Khoze and T. Sjostrand, Phys. Lett. B **274** (1992) 116; J. D. Bjorken, Phys. Rev. D **47** (1993) 101.
- [27] G. Marchesini, B. R. Webber, G. Abbiendi, I. G. Knowles, M. H. Seymour and L. Stanco, Comput. Phys. Commun. **67** (1992) 465.
- [28] R. Kuhn, A. Schaliche, F. Krauss and G. Soff, arXiv:hep-ph/0012025; S. Catani, F. Krauss, R. Kuhn and B. R. Webber, JHEP **0111** (2001) 063 [arXiv:hep-ph/0109231]; L. Lonnblad, JHEP **0205** (2002) 046 [arXiv:hep-ph/0112284]; F. Krauss, JHEP **0208** (2002) 015 [arXiv:hep-ph/0205283]; M.L. Mangano, presentation at the FNAL Matrix Element/Monte Carlo Tuning Working Group, 15 Nov 2002, <http://www-cpd.fnal.gov/personal/mreenna/tuning/nov2002/mlm.pdf>;

- S. Mrenna and P. Richardson, JHEP **0405** (2004) 040 [arXiv:hep-ph/0312274];
N. Lavesson and L. Lonnblad, JHEP **0507** (2005) 054 [arXiv:hep-ph/0503293].
- [29] F.E. Paige and S.D. Protopopescu, in *Physics of the SSC*, Snowmass, 1986, Colorado, edited by R. Donaldson and J. Marx.
- [30] V. D. Barger, R. J. N. Phillips and D. Zeppenfeld, Phys. Lett. B **346** (1995) 106 [arXiv:hep-ph/9412276].